# Aqueous Mechano-Bactericidal Action of Acicular Aragonite Crystals

**Nobuaki Negishi** ( n-negishi@aist.go.jp )
National Institute of Advanced Industrial Science and Technology
**Tomohiro Inaba**
National Institute of Advanced Industrial Science and Technology
**Yukari Miyazaki**
National Institute of Advanced Industrial Science and Technology
**Genki Ishii**
Chiba Institute of Technology
**Yang Yingnan**
University of Tsukuba
**Setsuko Koura**
Chiba Institute of Technology

**Research Article**

**Keywords:** Mechano-Bactericidal, Aragonite Crystals, synergistic bactericidal

**Posted Date:** June 10th, 2021

**DOI:** https://doi.org/10.21203/rs.3.rs-590395/v1

# Abstract

Nanoneedle structures on dragonfly and cicada wing surfaces or black silicon nanoneedles demonstrate antibacterial phenomena, namely mechano-bactericidal action. These air-exposed, mechano-bactericidal surfaces serve to destroy adherent bacteria, but their bactericidal action in the water is no precedent to report. Calcium carbonate easily accumulates on surfaces during long-term exposure to hard water. We expect that aragonite nanoneedles, in particular, which grow on $TiO_2$ during the photocatalytic treatment of calcium-rich groundwater, exhibit mechano-bactericidal action against bacteria in water. Here, we show that aragonite nanoneedles are grown on $TiO_2$ ceramics from the calcium bicarbonate in mineral water exhibit mechano-bactericidal action against *E. coli K-12* in water. Unmodified, calcite-modified as references and aragonite-modified $TiO_2$ ceramics were exposed to water containing *E. coli K-12* (in a petri dish), and their bactericidal action over time was investigated under static and agitated conditions. The surfaces of the materials were observed by scanning electron microscopy, and the live/dead bacterial cells were observed by confocal laser scanning microscopy. Further, the synergistic bactericidal performance achieved by mechano-bactericidal action and photocatalysis was demonstrated. Aragonite itself has a high biological affinity for the human body different from the other whisker-sharpen nano-materials, therefore, the mechano-bactericidal action of acicular aragonite in water is expected to inform the development of safe water purification systems for use in developing countries.


# Introduction

It was recently revealed that the surfaces of dragonflies, cicada wings, and the skins of geckos feature nanoneedle structures that show antibacterial activity[1–6]. Reported artificial reproductions of these structures, biomimetic structures, demonstrate similar antibacterial activity, known as the mechano-bactericidal effect[7–17]. Studies are steadily elucidating these mechano-bactericidal mechanisms. The main consequences of mechano-bactericidal actions are the sterilization of solid surfaces and the inhibition of biofilm formation. A significant advantage of the mechano-bactericidal mechanism is the absence of chemical reagents; this property of nanoneedle biomimetic structures is garnering the attention of scientists for their potential to feature in environmentally friendly and sustainable bactericidal technologies.

Natural water typically contains various mineral components. Many are familiar with the white precipitate (scale) that forms and adheres to faucets; it develops when the concentrations of certain mineral components in tap water are relatively high. This white precipitate is calcium carbonate, with the crystal structure of mainly aragonite or calcite; significantly, aragonite has a needle crystal habit[18]. In a previous study, we found that calcium carbonate forms on the surface of $TiO_2$ photocatalysts during the photocatalysis of calcium bicarbonate in water. Moreover, the calcium carbonate mainly demonstrates the crystallinity of aragonite with nano– to micrometer–sized needles[19]. We expected that these aragonite nanoneedles would continuously kill any bacteria in flowing water upon contact through the mechano-bactericidal action associated with their topography. As mentioned above, most studies on

mechano-bactericidal effects are at the air-solid interface, and reports on mechano-bactericidal effects for bacterial treatment in water are almost impossible to find. It would be a new discovery if the aragonite needle crystal has a mechano-bactericidal effect in the water.

The mechano-bactericidal action of acicular aragonite in water will be expected to inform the development of water purification systems for use in developing countries, therefore, we studied the mechano-bactericidal action of aragonite nanoneedles against *Escherichia coli (E. coli) K-12* in the water phase.

# Results And Discussion

The aragonite nanoneedles are immobilized on stable $TiO_2$ ceramic[20]. For comparison, we also evaluated the bactericidal action of unmodified $TiO_2$ ceramic and calcite nanocrystals immobilized on $TiO_2$ ceramic against *E. coli K-12*. The bactericidal evaluations were based on two experimental procedures. In the first procedure, water loaded with *E. coli K-12* was poured into a petri dish containing aragonite-modified (or calcite-modified) $TiO_2$ ceramic and maintained for a maximum of 16 h under static and agitated conditions. The second experiment involved a closed circulation system, used to simulate actual conditions, featuring a $TiO_2$ ceramic monolith–packed Pyrex glass tube (300 mm × 10 mm (internal diameter)). In this system, we observed a decrease in the number of *E. coli K-12* cells in water as a function of circulation time. The *E. coli K-12* cells on the surface of aragonite-modified (or calcite-modified) $TiO_2$ ceramic were observed by confocal laser scanning microscopy.

Calcium carbonate accumulates on the $TiO_2$ ceramic surface, as shown in Fig. 1, during the long-term circulation of mineral water containing calcium bicarbonate under UV irradiation. Mineral water containing only calcium bicarbonate produces a precipitate characterized by hexagonal crystals, while mineral water (such as Evian® and Contrex®) containing magnesium and strontium ions along with calcium bicarbonate produces a precipitate characterized by acicular crystals (Fig. 2). The X-ray diffraction (XRD) and laser-Raman spectra in Fig. 3, respectively, reveal that the crystal structures of the hexagonal and acicular calcium carbonate are calcite and aragonite, respectively.

Acicular aragonite crystals do not form on the $TiO_2$ ceramic surface when water is circulated over the photocatalyst in the absence of UV irradiation. Whereas, under UV irradiation, bicarbonate ions are converted to carbonate ions by photocatalysis to form insoluble acicular calcium carbonate, i.e., aragonite, on the $TiO_2$ ceramic surface. The lengths of the acicular crystals range from 10 nm to a few micrometers, depending on the duration of circulation and the concentration of calcium bicarbonate in the mineral water. It is expected that the large (micrometer) acicular crystals will capture the bacteria in a water-flow system, while the small (sub-micrometer) acicular crystals exert a mechano-bactericidal effect.

The changes in the number of *E. coli K-12* cells in an aqueous phase over time are shown in Fig. 4. The number of *E. coli K-12* cells does not change significantly in a saline water system. In a system containing unmodified $TiO_2$ ceramics, the number of *E. coli K-12* cells decreases slightly. Finally, in a

system containing aragonite-modified $TiO_2$, the number of *E. coli K-12* cells decreases remarkably. The decrease in the number of bacterial cells under static conditions indicates that *E. coli K-12* is captured by acicular aragonite owing to its own motor function, and the improvement in the antibacterial action achieved by agitation is less significant than the antibacterial action associated with the motor function of the bacteria.

Figure 5 display SEM images of the surfaces of unmodified, calcite-modified, and aragonite-modified $TiO_2$ ceramics that were immersed in saline water containing *E. coli K-12* for 16 h. The distinctive shapes of *E. coli K-12* cells on the unmodified (Fig. 5 (1)) and calcite-modified $TiO_2$ ceramic surfaces (Fig. 5 (2) and (2')) do not change after 16 h; in contrast, the distinct shapes of *E. coli K-12* cells are absent on the aragonite-modified $TiO_2$ ceramic surfaces. In Figs. 5(3) and 5(3'), the cell membrane was observed to be stretched and leathery. In Fig. 5(3"), a situation was observed in which a substance that appeared to be protoplasm was ejected from the stab wounds of E. coli.

Figure 6 show images of live/dead *E. coli K-12* cells on naked $TiO_2$ ceramic (a) and aragonite-modified $TiO_2$ ceramics (b) obtained by confocal microscopy after 16 h in an *E. coli K-12* solution under static condition ($5 \times 10^3$ CFU/mL). The green color indicates viable cells, and the red color indicates dead cells. The number of cells (dead and alive) on the aragonite-modified $TiO_2$ ceramic surface was much smaller than the number of cells on the unmodified $TiO_2$ ceramic surface. However, the small number of dead cells observed suggests that the nucleic acid, which is stained with a fluorescent dye, eluted into the aqueous phase through the punctured cell wall (impaled by acicular aragonite: as shown in Fig. 5(3")); this loss of nucleic acid (and fluorescent marker) accounts for the low incidence of cells (dead) observed by confocal microscopy on the aragonite-modified $TiO_2$ ceramic surface.

The fate of bacteria captured by nanoneedle structures has already been reported. Hazel et al. and Jenkins et al. found that nanoneedles penetrate the cell membranes of bacteria[11, 25], resulting in sterilization. Wu et al. considered the relationship between the length of the nanoneedle that penetrates the bacterial-cell wall and the inter-needle distance[9]. They reported that the stretching of the cell membrane increases with the increasing density of the nanoneedles. Their experiment investigated the bacteria at the gas–solid interface; however, we expect that the mechano-bactericidal mechanism at the gas–solid interface should be similar to that at the liquid–solid interface in this study because we observed bacteria impaled on the acicular aragonite.

Therefore, we investigated the mechano-bactericidal performance of acicular aragonite with different nanoneedle sizes. As shown in Fig. 7, the mechano-bactericidal performance of acicular aragonite was dependent on the size of the nanoneedles. That is, the mechano-bactericidal action of acicular aragonite characterized by small needles with a length and diameter of 1–2 and 0.05–0.1 μm, respectively, is high; while that of acicular aragonite characterized by larger needles with a length and diameter of 2–6 and 0.2–0.6 μm, respectively, is low. This needle-size dependence of mechano-bactericidal performance is consistent with the results of earlier studies for the gas-sold phase[7, 9, 11, 17, 21].

Figure 8 reveals the mechano-bactericidal action in circulation systems. Unmodified, calcite-modified, and aragonite-modified $TiO_2$ ceramics were packed into Pyrex glass tubes (300 mm × 10 mm (internal diameter)) and water containing *E. coli K-12* ($5 \times 10^3$ CFU/mL) were circulated through these tubes at a rate of 50 mL/min. Figures 3a, 3b, and 3c show images of the live/dead *E. coli K-12* cells on the surfaces of the unmodified, calcite-modified, and aragonite-modified $TiO_2$ ceramics, respectively, after circulating the aqueous phase for 3 h. A significant amount of viable *E. coli K-12* cells is observed on the surface of the unmodified $TiO_2$ ceramics (Fig. 8 (a)). The total number of bacterial cells on the surface of the calcite-modified $TiO_2$ ceramics (Fig. 8 (b)) is less than that on the surface of the unmodified $TiO_2$ ceramics; however, both viable and dead bacteria are observed. As shown in Fig. 8 (c), very few dead bacterial cells are observed on the surface of the aragonite-modified $TiO_2$ ceramics, despite the presence of viable bacteria; this result is consistent with the result obtained under static conditions (Fig. 6).

The most significant finding of this research is the aqueous mechano-bactericidal action of aragonite consisting of calcium carbonate. Almost all of the reported nanoneedle, nanopillar, and whisker-shaped materials exhibit mechano-bactericidal action. However, it is known that asbestos, potassium titanate, carbon nanotubes, and metal nanowires demonstrate lung toxicity due to oxidative stress induced by their shape[22–24]. Acicular aragonite consists of nanoneedle-shaped crystals as well and its associated toxicity is still subject to further study. However, acicular aragonite does not show toxicity toward lung tissue, unlike the aforementioned nanoneedle, nanopillar, and whisker-shaped materials[18]. Calcium carbonate, which is the main component of aragonite, easily dissolves in the human body and, as a result, morphology-induced toxicity does not manifest. In the course of water treatment through the mechano-bactericidal action of aragonite-modified $TiO_2$ ceramics, we must assume the defluxion of nanoneedles into the water as a result of fracturing. Unlike body-soluble acicular aragonite, nanoneedle, nanopillar, and whisker-shaped nanomaterials are unsuitable for drinking water treatment because of the risk of fragment effluence.

We have already mentioned the possibility of damage to acicular aragonite during water treatment; however, it is also expected that the acicular aragonite will recover/self-repair in natural water flow. More specifically, the self-replication ability of the system, and its mechano-bactericidal action, is anticipated. In fact, we found that acicular aragonite nucleates from dead *E. coli K-12* cells during long-term circulation (Fig. 9).

Photocatalytic environmental purification can only be performed during the daytime and, for optimum performance, under sunny conditions[26–28]. However, ideal photocatalytic drinking-water purification systems for developing countries should achieve absolute performance under all weather conditions, not only sunny but also cloudy or rainy; possibly by combining photocatalytic activity and mechano-bactericidal action. Figure 10 shows the change in number of *E. coli K-12* cells in circulation systems featuring tubes containing unmodified and aragonite-modified $TiO_2$ ceramics under dark and UV light conditions. The number of *E. coli K-12* cells in the unmodified $TiO_2$ ceramic system decreases significantly more under UV-A irradiation than dark conditions due to photocatalysis[29,30]. However, the

number of *E. coli K-12* cells in the aragonite-modified $TiO_2$ ceramic system under dark conditions is lower than that in the unmodified $TiO_2$ ceramic system under UV-A irradiation. Significantly, the absolute rate of *E. coli K-12* cell reduction in the aragonite-modified $TiO_2$ ceramic system under UV-A irradiation (Sterilization rate const. = 1.22 $h^{-1}$) was ~ 2.0 times of under dark (Reduction rate const. = 0.809 $h^{-1}$), and ~ 3.0 times of the UV light conditions in the unmodified $TiO_2$ ceramic system (Photocatalytic rate const. = 0.618 $h^{-1}$).

In a previous study, we revealed why the photocatalytic activity of $TiO_2$ does not decrease with increasing aragonite accumulation on its surface[19]. The photocatalytic reaction mainly involves the formation and migration of active species, such as •OH, by UV irradiation of the $TiO_2$ photocatalyst. The lifetime of •OH, of around 2.7 μs[38], is considered sufficient to allow it to migrate into the aqueous phase through the layer of aragonite. The densification of the aragonite layer is expected to impede the migration of active species. In reality, the aragonite layer on the $TiO_2$ surface is very porous and a few micrometers thick. This porosity facilitates the migration of the active species, generated by photocatalysis, to the surface of the aragonite layer. This is one of the reasons why the photocatalytic sterilization performance of the aragonite-modified $TiO_2$ ceramic photocatalyst exceeds that of the unmodified $TiO_2$ ceramic photocatalyst. Moreover, the mineralization of bacteria on the aragonite-modified $TiO_2$ ceramic photocatalyst is promoted by photocatalysis; as a result, the surface of this material will maintain a clean condition unlike that of an aragonite system without photocatalytic materials.

As described above, we demonstrated the mechano-bactericidal treatment of water by acicular aragonite. However, several aspects require elucidation, such as the relationship between the optimum needle size of aragonite or flow speed and bactericidal performance, and the mechano-bactericidal action of acicular aragonite against other bacterial species. As previously reported, the $TiO_2$ ceramic photocatalyst, which is used as a substrate for acicular aragonite growth, is extremely strong and does not deteriorate during long-term use. Therefore, it is expected that access to safe water can be achieved in many developing countries with systems that combine mechano-bactericidal action and photocatalysis, such as the proposed acicular aragonite-modified $TiO_2$ ceramic system, that obviate the use of disinfectants and concomitant chemical risks and high running costs.

# Conclusion

Acicular aragonite nano-needle, a metastable phase of calcium carbonate, precipitated on the photocatalytic surface by the photocatalytic reaction of calcium bicarbonate contained water such as ground water, showed a mechano-bactericidal effect in water which is not still known. Calcite, which is a stable phase of calcium carbonate, did not show any mechano-bactericidal effect. From the results of phase contrast microscopy, the aragonite phase showed a low density of dead bacteria on its surface, which may be due to the leakage of protoplasm to be stained into the water. Although the mechano-bactericidal effect alone was greater than the photocatalytic effect alone, the synergistic effect was observed for the aragonite modified photocatalyst, and the bactericidal rate in water was equal to the

sum of the mechano-bactericidal and photocatalytic effects. The aragonite modified photocatalyst is expected to be used for drinking water purification in developing countries, the loss of aragonite needle crystal habit may occur due to its long-term use. However, it was confirmed that aragonite was precipitated from dead bacteria after long-term use of the aragonite modified photocatalyst in hard water, indicating that the material has a self-regenerating function to maintain its mechano-bactericidal effect and is a promising material for realizing safe water access in developing countries. The results showed that this material has a self-renewal function to maintain its mechano-bactericidal effect and is a promising material for achieving safe water access in developing countries.

## Methods

## Substrates for $CaCO_3$ growth

The preparation of a $TiO_2$ ceramic photocatalyst employed as a substrate for the growth of $CaCO_3$ crystals, such as aragonite, has previously been reported[19]. $TiO_2$ is known as a photocatalytic material that has two crystal phases, anatase and rutile. The photocatalytic activity of anatase is high, higher than that of rutile[31–33]. Unless specified otherwise, all of the experimental procedures were carried out in the absence of UV light; in particular, we used high temperature treated (750°C) rutile $TiO_2$ ceramic as a substrate for aragonite immobilization to reduce the risk of undesired photocatalytic reactions. On the other hand, anatase $TiO_2$ ceramics calcined at 550°C were used in the photocatalytic (under UV irradiation) experiments. This ceramic photocatalyst is generally more robust in water than other photocatalytic materials and, since its semipermanent use in the water is expected, very suitable for the treatment of drinking water in developing countries[20].

### Growth Of Aragonite And Calcite On Tio Ceramic Surfaces

Commercial mineral water is the most suitable starting material for the growth of acicular aragonite crystals on $TiO_2$ ceramics. Certain brands of mineral waters are rich in calcium bicarbonate (as indicated by their ingredients labels of commercial products). While these mineral waters contain various minerals, only one precipitate, calcium carbonate, is generally formed. We used Contrex® from France since this mineral water contains high concentrations of calcium bicarbonate and its pH is almost neutral. In contrast, the precipitation of a calcite reference sample requires a pure calcium bicarbonate solution. The calcium bicarbonate solution employed in this study was the filtrate of a solution prepared by bubbling $CO_2$ gas through a calcium hydroxide–saturated solution[34]. To grow aragonite (or calcite) on $TiO_2$ ceramics, 500 mL of Contrex® (or calcium bicarbonate solution) was introduced into a water flow line connected to a glass tube packed with $TiO_2$ ceramics under UV irradiation. The circulatory system is the same as in our previous report[19]. After circulating for 8 h, the circulation system and content were dried under airflow for 16 h; this circulation and drying process was repeated 15 times. The crystalline structures of these precipitates were determined using X-ray diffraction (XRD; D2 Phaser, Bulker Germany) and laser Raman spectroscopy (NRS-4500, JASCO, Tokyo, Japan). The morphologies of the surfaces of

these materials were observed by field emission scanning electron microscopy (FE-SEM; S-4700, Hitachi, Tokyo, Japan) [35].

## Biological Experiments

*E. coli K-12*, purchased from NITE Biological Resource Center (NBRC No. 3301) as a model bacterium, was streak-cultured on an agar plate (NBNaCl medium: Bacto Peptone (Becton, Dickinson and Company, NJ, USA) 0.5%, beef extract(MP Biomedicals LLC, CA, USA) 0.3%, NaCl 0.5%, agar(FUJIFILM Wako Pure Chemical Corporation, Osaka, Japan) 1.5%), and then shake cultured at 60 rpm in liquid NBNaCl medium containing Bacto Peptone 0.5%, beef extract 0.3%, and NaCl 0.5% at 36°C for 16 h. The *E. coli K-12* growth curve was determined from the optical density at 600 nm measured with a cell density meter (CO8000, Biochrom, Cambridge, UK). The *E. coli K-12* was cultured until the system reached a stationary state at 0.5–1 × $10^8$ CFU/mL. The cultured *E. coli K-12* was diluted once with phosphate-buffered saline, and 0.1 mL of the diluted/undiluted culture was used to inoculate the NBNaCl culture media plates. The *E. coli* was cultured on the NBNaCl media at 35°C for 24 h.

The number of colonies was counted using a colony counter and the average number of colonies was calculated. If the number of colonies per dilution factor differed by more than a factor of 2, the value for the culture medium with a lower dilution factor was used. All media, incubation flasks, micropipette tips, and filtration units (including bottle parts used for the preparation of bacterial suspensions) were sterilized by autoclaving at 121°C for 20 min or by gamma sterilization.

## Mechano-bactericidal Experiment (Incl. Photocatalysis)

To analyze the mechano-bactericidal action of the materials, we performed one type of static and two types of dynamic experiments. In the static experiment, cultured *E. coli K-12* (1 × $10^7$–$10^8$ CFU/mL) solution was fed into culture tubes (volume: 5 mL), containing one piece of unmodified $TiO_2$ ceramic, calcite-modified $TiO_2$ ceramic, or aragonite-modified $TiO_2$ ceramic, that was then left at rest at 4°C for 16 h. The *E. coli K-12* cells on the surface of each substrate were observed by confocal microscopy, after staining the cells with SYTO9 and PI, to estimate the live/dead bacterial cell abundance and evaluate their membrane integrity. In addition, the *E. coli K-12* cells on the aragonite-modified $TiO_2$ ceramic surface were observed by FE-SEM after fixation with glutaraldehyde[36, 37].

The first dynamic experiment was a time–course experiment; 50 mL of a solution containing *E. coli K-12* (~ 5000 CFU/mL) was poured into petri dishes containing unmodified or aragonite-modified $TiO_2$ ceramics and sampling was performed every 30 min for 3 h at 25 ºC under static and agitated conditions in a shaking incubator. For reference, this procedure was repeated without any substrates (blank). The initial number of *E. coli K-12* cells in the respective samples, determined by confocal microscopy, differ from each other and from the initial bacterial solution concentration (~ 5000 CFU/mL). These differences are attributed to the different culture methods employed and the detection limits of confocal microscopy associated with these culture methods.

In the second dynamic experiment, to simulate a practical application, we circulated 250 mL of saline water (0.5 g/L) containing *E. coli K-12* (5000 CFU/mL) through a glass tube packed with aragonite-modified $TiO_2$ ceramics for 3 h at a flow rate of 50 mL/min. We also used the black-light blue fluorescent lamp (15W-BLB) for photocatalytic reaction as the light source when the photocatalytic experiment was carried out, and the UV-A (l = 365 nm) intensity was fixed at 2 $mW/cm^2$ at the position of the photocatalyst-packed tube. The UV-A intensity was measured by means of a UV power meter C9356-1 (Hamamatsu Photonics, Hamamatsu, Japan).

The solution was sampled every 30 min, and 0.1 mL of each sample was used to inoculate the NBNaCl culture media plates and cultured at 35°C for 24 h. After each 3-hour circulation, the apparatus was drained under air pressure and disinfected by circulating ethanol (FUJIFILM Wako Pure Chemical Corporation, Osaka, Japan) for two 30-min periods. Milli-Q water was passed through (not circulated) the apparatus for 2 h; the apparatus was again drained under air pressure before the aragonite-modified $TiO_2$ ceramics in the apparatus was dried overnight under flowing air and UV irradiation (λ = 352 nm) to eliminate any residual organic compounds and bacteria on the surface of the $TiO_2$ by photocatalysis. After the circulation experiment, aragonite-modified $TiO_2$ ceramic was abstracted from the glass tube and the bacteria were observed by FE-SEM after fixation with glutaraldehyde.

## Declarations


# Declarations


### Competing interests

The authors declare no competing interests.

# Contributions

G.I. prepared the materials, performed the biological experiment and surface analyses. Y. M. performed the biological experiment. T.I. performed the analyses. Y. Y. and K. S. participated in the discussion of bactericidal performance. N.N. directed and supervised the study and the project. N.N. wrote the main text of the manuscript. All authors contributed to the discussion and reviewed the manuscript.

# Acknowledgements


This work was supported by A-STEP Tryout program (Grant No. 21-201031976) from the Japan Science and Technology Agency (JST).


# Affiliations

1 Environmental Management Research Institute, National Institute of Advanced Industrial Science and Technology (AIST), 16-1 Onogawa, Tsukuba 305-8569, Japan 2 Department of Applied Chemistry, Chiba Institute of Technology, 2-17-1 Tsudanuma, Narashino 275-0016, Japan 3 Graduate School of Life and Environmental Science, University of Tsukuba, 1-1-1 Tennodai, Tsukuba, Ibaraki 305-8572, Japan

# References

1. Ivanova, E. P. *et al*. Natural bactericidal surfaces: mechanical rupture of Pseudomonas aeruginosa cells by cicada wings. *Small* **8**, 16, 2489–2494 (2012).
2. Hasan, J. *et al*. Selective bactericidal activity of nanopatterned superhydrophobic cicada *Psaltoda claripennis* wing surfaces. *Environ. Biotechnol.* **97**, 9257–9262 (2013).
3. Ivanova, E. P. *et al*. Bactericidal activity of black silicon. *Nat. Commun.* **4**, 2838 (2013).
4. Watson, G. S. *et al*. A gecko skin micro/nano structure – A low adhesion, superhydrophobic, anti-wetting, self-cleaning, biocompatible, antibacterial surface. *Acta Biomater.* **21**, 109–122 (2015).
5. Linklater, D. P., Juodkazis, S., Ivanova, E. P. Nanofabrication of mechano-bactericidal surfaces. *Nanoscale* **9**, 16564–16585 (2017).
6. Cheesman, S. *et al*. Interaction of giant unilamellar vesicles with the surface nanostructures on dragonfly wings. *Langmuir* **35**, 2422–2430 (2019).
7. Tripathy, A., Sen, P., Su, B., Briscoe, W. H. Natural and bioinspired nanostructured bactericidal surfaces. *Adv. Colloid Interface Sci.* **248**, 85–104 (2017).
8. Green, D. W. *et al*. High quality bioreplication of intricate nanostructures from a fragile gecko skin surface with bactericidal properties. *Sci. Rep.* **7**, 41023 (2017)
9. Wu, S., Zuber, F., Maniura–Weber, K., Brugger, J., Ren, Q. Nanostructured surface topographies have an effect on bactericidal activity. *J. Nanobiotechnol.* **16**, 20 (2018).
10. May, P. W. *et al*. Diamond-coated 'black silicon' as a promising material for high-surface-area electrochemical electrodes and antibacterial surfaces. *J. Mater. Chem. B* **4**, 5737–5746 (2016).
11. Hazell, G. *et al*. Studies of black silicon and black diamond as materials for antibacterial surfaces. *Biomater. Sci.* **6**, 1424–1432 (2018).
12. Bhada, C. M. *et al*. Subtle variations in surface properties of black silicon surfaces influence the degree of bactericidal efficiency. *Nano-Micro Lett*. **10**, 36 (2018).
13. Wandiyanto, J. *et al*. The fate of osteoblast-like MG-63 cells on pre-infected bactericidal nanostructured titanium surfaces. *Materials* **12**, 1575 (2019).
14. Tan, Q., Lu, F., Zue, C., Zhang, W., Lin, L. Nano-fabrication methods and novel applications of black silicon. *Sensor. Actuator. A: Phys.* **295**, 560–573 (2019).
15. Wandlyanto, J. V. *et al*. Outsmarting superbugs: bactericidal activity of nanostructured titanium surfaces against methicillin- and gentamicin-resistant *Staphylococcus aureus* ATCC 33592. *J. Mater. Chem. B* **7**, 4424–4431 (2019).

16. Wandlyanto, J. V. *et al*. Tunable morphological changes of asymmetric titanium nanosheets with bactericidal properties. *J. Colloid. Interface Sci.*, **560**, 572–580 (2020).
17. Nguyen, D. H. *et al*. The idiosyncratic self-cleaning cycle of bacteria on regularly arrayed mechano-bactericidal nanostructures. *Nanoscale* **11**, 16455–16462 (2019).
18. Horie, M. *et al*. Comparison of proinflammatory potential of needle-shaped materials: aragonite and potassium titanate whisker. *Arch. Toxicol.* **93**, 2797–2810 (2019).
19. Negishi, N., Miyazaki, Y., Kato, S., Yang, Y. Effect of $HCO_3^-$ concentration in groundwater on $TiO_2$ photocatalytic water purification. *Appl. Catal. B: Environ.* **242**, 449–459 (2019).
20. Kato, S. *et al*. Development of monolithic titanium dioxide ceramic photocatalysts with high physical rigidity and photocatalytic activity for underwater use. *Ceram. Int.* **46**, 19285–-19292 (2020).
21. Jenkins, J. *et al*. Antibacterial effects of nanopillar surfaces are mediated by cell impedance, penetration and induction of oxidative stress. *Nat. Commun.* **11**, 1626 (2020).
22. Rahman, L. *et al*. Multi-walled carbon nanotube-included genotoxic, inflammatory and profibrotic response in mice: Investigating the mechanisms of pulmonary carcinogenesis. *Mutat. Res. Gen. Tox. En.* **823**, 28–44 (2017).
23. Kane, A. B., Hurt, R. H., Gao, H. The asbestos-carbon nanotube analogy: an update. *Tox. Appl. Pharmacol.* **361**, 68–80 (2018).
24. Abdelgied, M. *et al*. Potassium octatitanate fibers induce persistent lung and pleural injury and are possibly carcinogenic in male Fischer 344 rats. *Cancer Sci.* **109**, 2164–2177 (2018).
25. Romero, M. *et al*. Solar photocatalytic degradation of water and air pollutants: challenges and perspectives. *Sol. Energy* **66**, 109–-182 (1999).
26. Sciacca, F., Rengifo-Herrera, J. A., Wéithe, J., Pulgarin, C. Solar disinfection of wild Salmonella sp. in natural water with a 18 L CPC photoreactor: detrimental effect of non-sterile storage of treated water. *Sol. Energy* **85**, 1399–1408 (2011).
27. Negishi, N., Sano, T. Photocatalytic solar tower reactor for the elimination of a low concentration of VOCs. *Molecules* **19**, 16624–16639 (2014).
28. Negishi, N., Chawengkijwanich, C., Pimpha, N., Larpkiattawom, S., Charipanitkl., T. Performance verification of the photocatalytic solar water purification system for sterilization using actual drinking water in Thailand. *J. Water Process Eng.* **31**, 100835 (2019).
29. Rincón, A. G., Pulgarin, C. Effect of pH, inorganic ions, organic matter, and $H_2O_2$ on E. coli K12 photocatalytic in solar water disinfection. *Appl. Catal. B Environ.* **51**, 283–302 (2004).
30. Gong, M. *et al*. Research process of photocatalytic sterilization over semiconductors. *RSC Adv.* **9**, 19278–19284 (2019).
31. Sclafani, A., Herrmann, J. M. Comparison of the photoelectronic and photocatalytic activities of various anatase and rutile forms of titania in pure liquid organic phases and in aqueous solutions. *J. Phys. Chem.* **100**, 13655–13661 (1996).

32. Ding, Z., Lu, G. Q., Greenfield, P. F. Role of the crystallite phase of $TiO_2$ in heterogeneous photocatalysis for phenol oxidation in water. *J. Phys. Chem. B* **104**, 4815–4820 (2000).
33. Yu, J. *et al*. Effect of calcination temperature on the surface microstructure and photocatalytic activity of $TiO_2$ thin films prepared by liquid phase deposition. *J. Phys. Chem. B* **107**, 13871–13879 (2003).
34. Chuajiw, W. *et al*. Effects of amine, amine salt and amide on the behaviour of carbon dioxide absorption into calcium hydroxide suspension to precipitate calcium carbonate. *J. Environ. Sci.* **25**(**12**), 2507–2515 (2013).
35. Musić, S. *et al*. Chemical and microstructural properties of $TiO_2$ synthesized by sol-gel procedure. *Materials Science and Engineering*, **B47**, 33–40 (1997).
36. Hayat, M. A. Glutaraldehyde: role in electron microscopy. *Micron and Microscopica Acta* **17**(**2**), 115–135 (1986).
37. Park, C., Kim, H., Rhyu, I., Uhm, C. How to get well-preserved samples for transmission electron microscopy. *Appl. Microsc.* **46**(**4**), 188–192 (2016).
38. Attri, P. et al. Generation mechanism of hydroxyl radical species and its lifetime prediction during the plasma-initiated ultraviolet (UV) photolysis. *Sci. Rep.*, DOI: 10.1038/srep09332 (2015).

# Figures

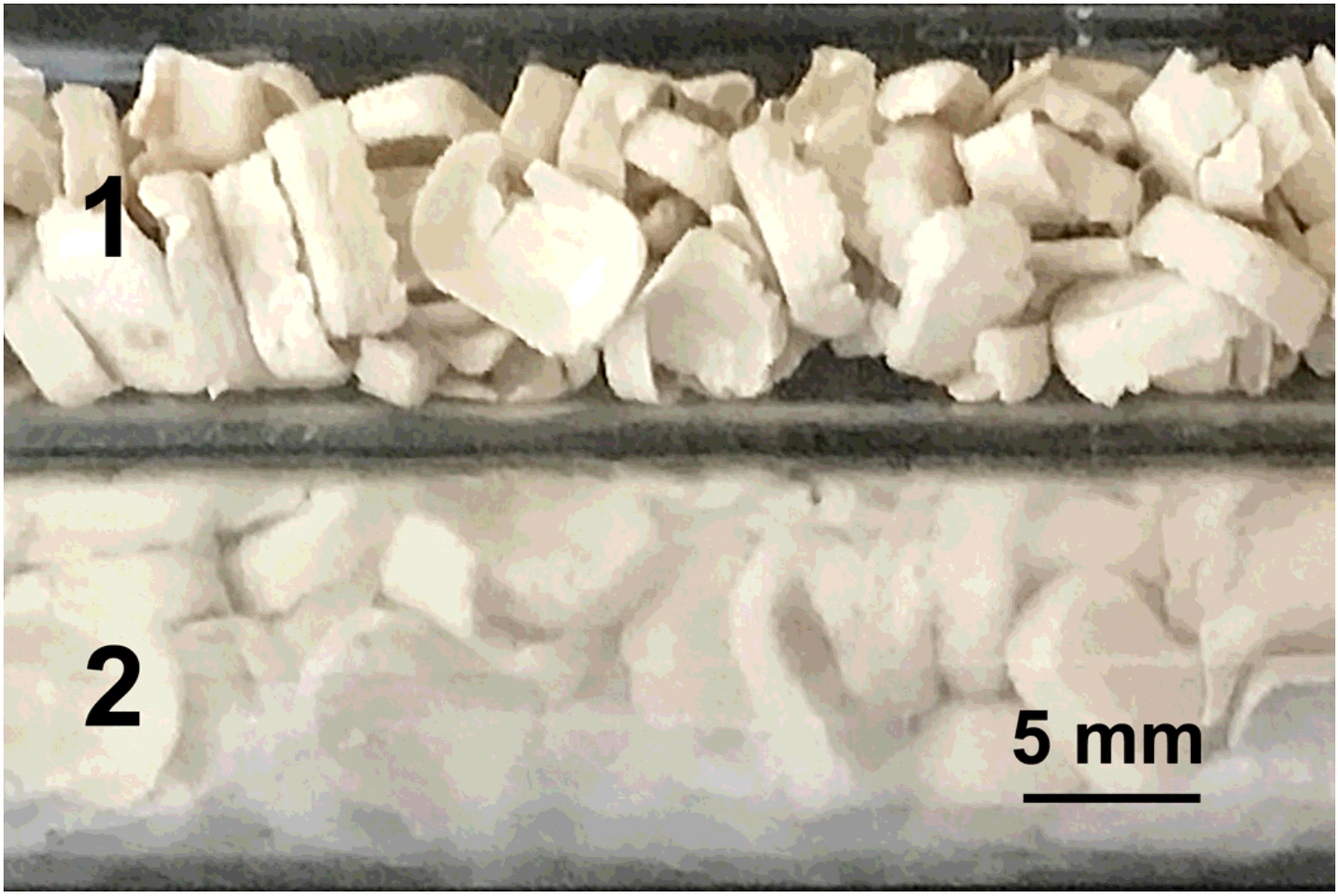


**Figure 1**

Formation of CaCO3 crystals on TiO2 ceramics. (1) Image of TiO2 ceramics (approximate dimensions: 5 mm × 3 mm × 1 mm) and (2) calcium carbonate accumulated TiO2 ceramics.

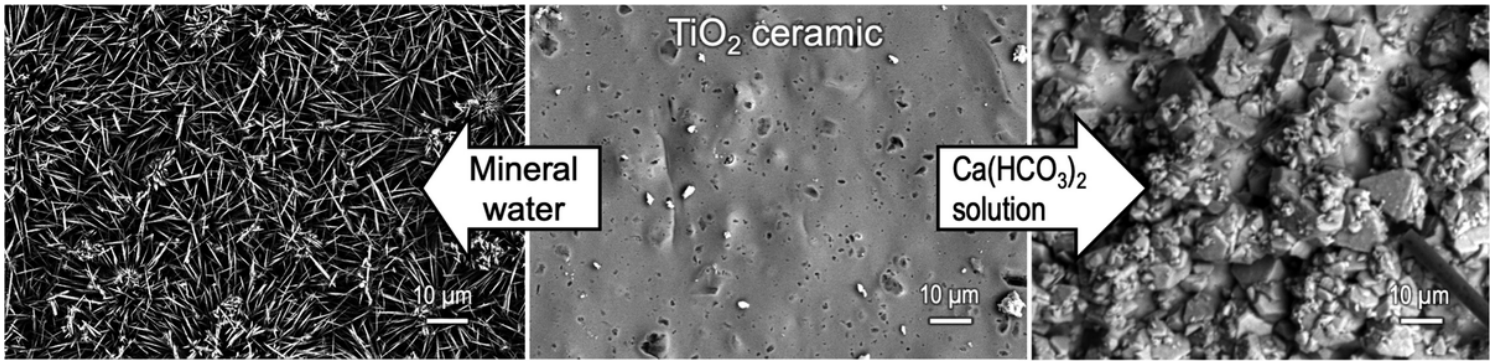


**Figure 2**

SEM images of modified (center) and unmodified TiO2 ceramic surfaces by CaCO3 (left: TiO2 modified during mineral water circulation, right: TiO2 modified during Ca(HCO3)2 circulation).

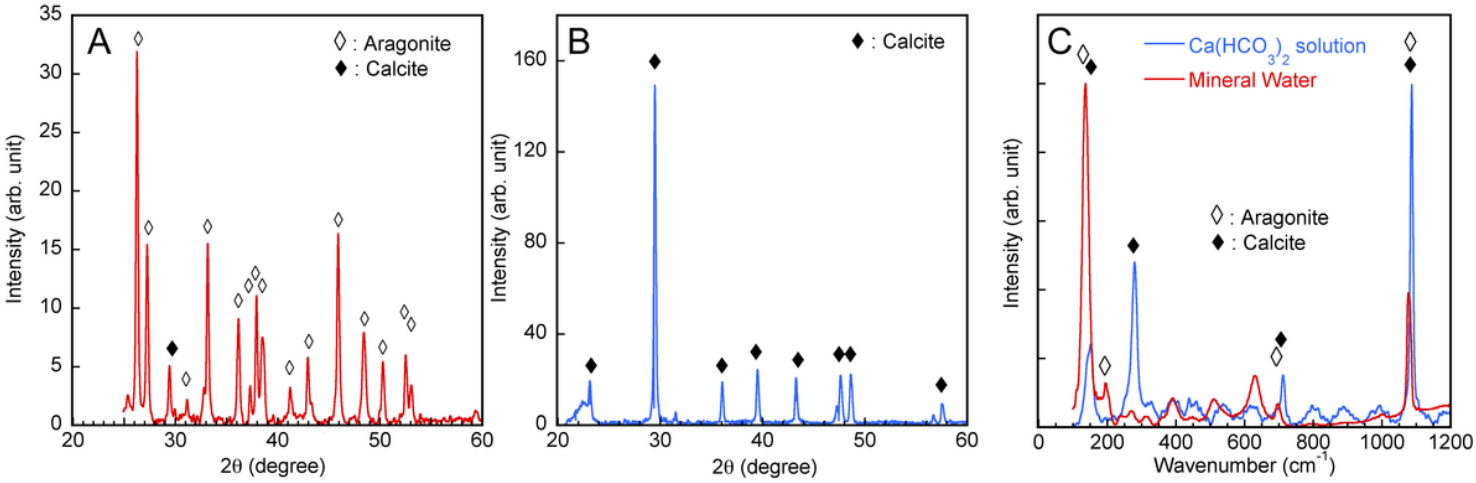


## Figure 3

XRD spectra of crystals precipitated from mineral water (a) and a Ca(HCO3)2 solution (b), and Laser-Raman spectra of crystals precipitated from mineral water and a Ca(HCO3)2 solution (c).

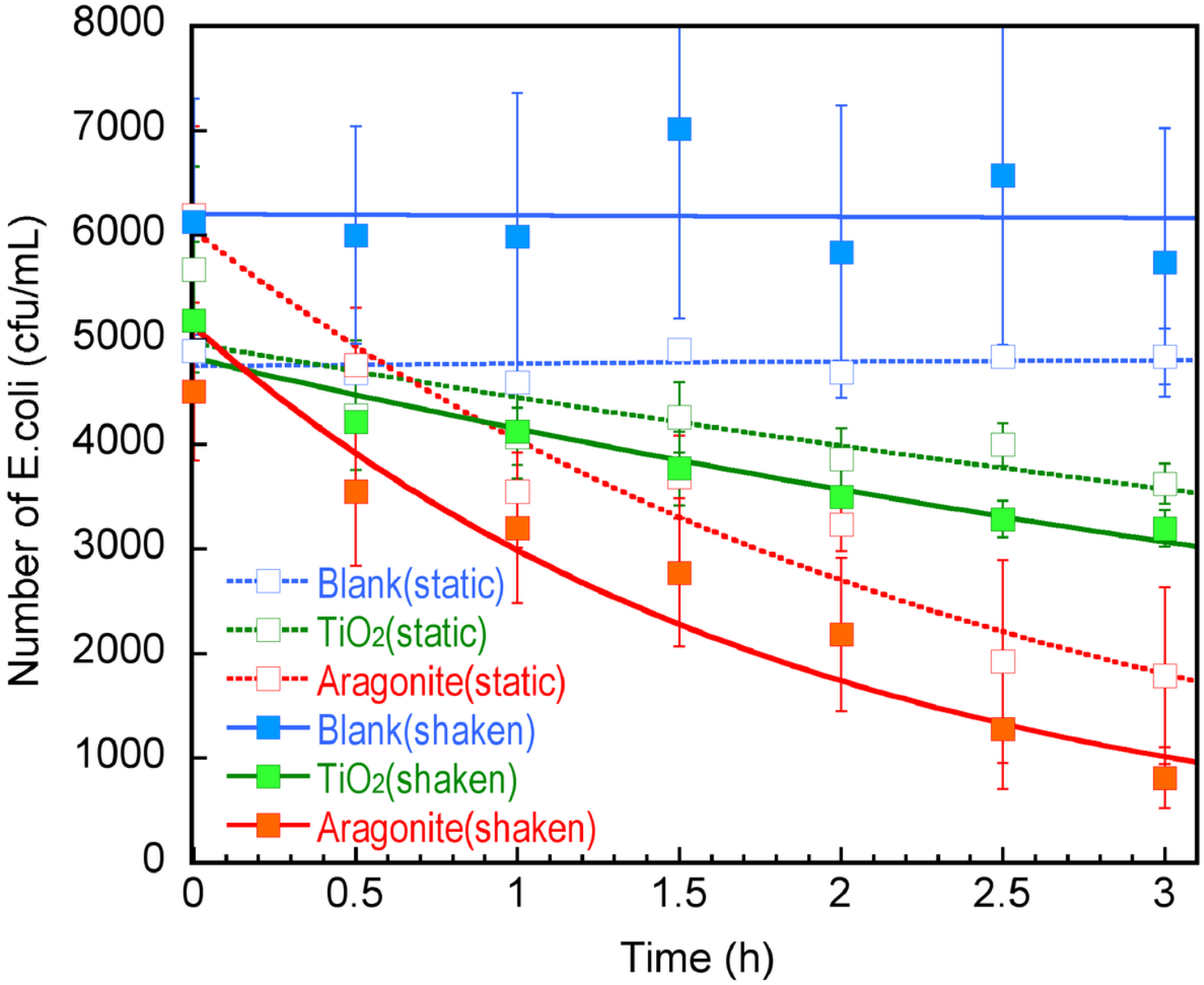


**Figure 4**

Changes in the number of underwater E. coli K-12 on unmodified and CaCO3-modified TiO2 ceramics under static conditions.

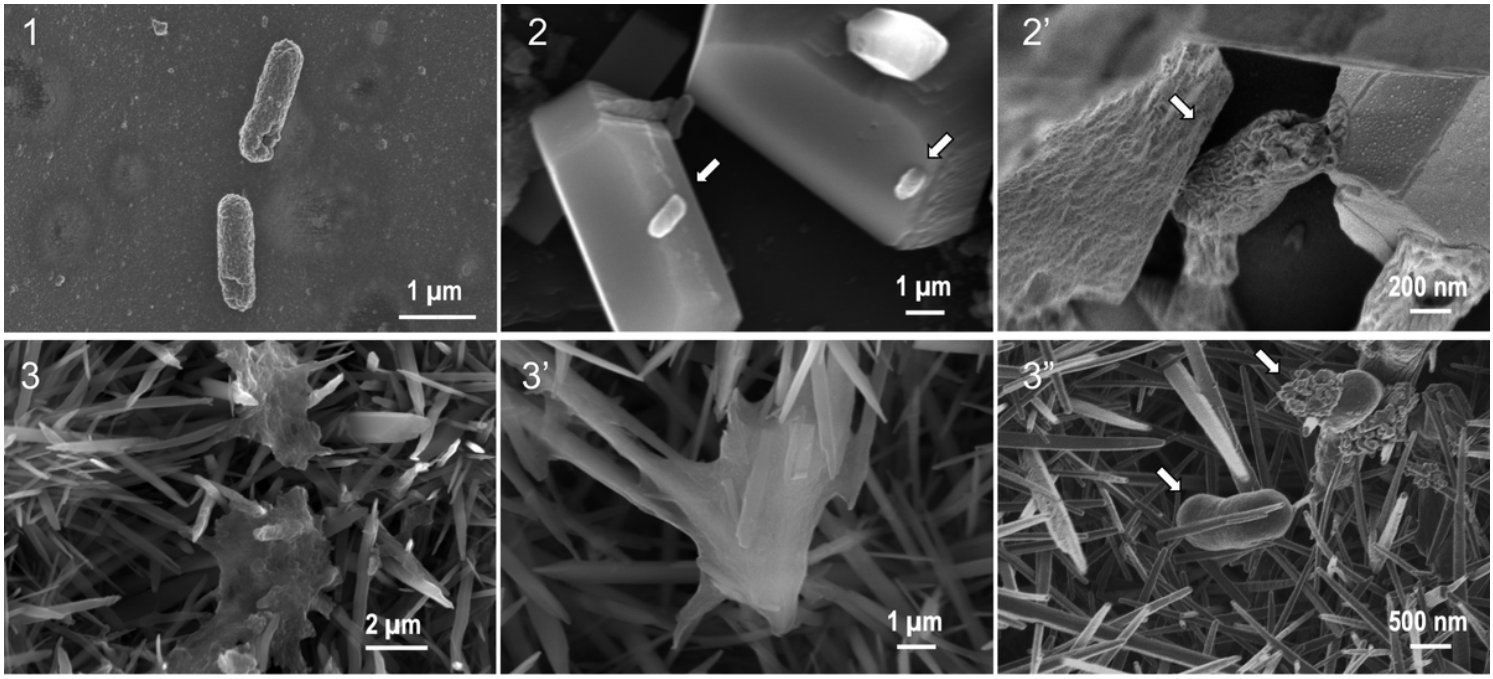


## Figure 5

SEM image of E. coli K-12 cells on a TiO2 ceramic surface (1). SEM images of E. coli K-12 cells on calcite-modified TiO2 ceramic surfaces under low (2) and high (2') magnification. SEM images of E. coli K-12 cells on aragonite-modified TiO2 ceramic surfaces under low (3), middle (3'), and high (3") magnification.

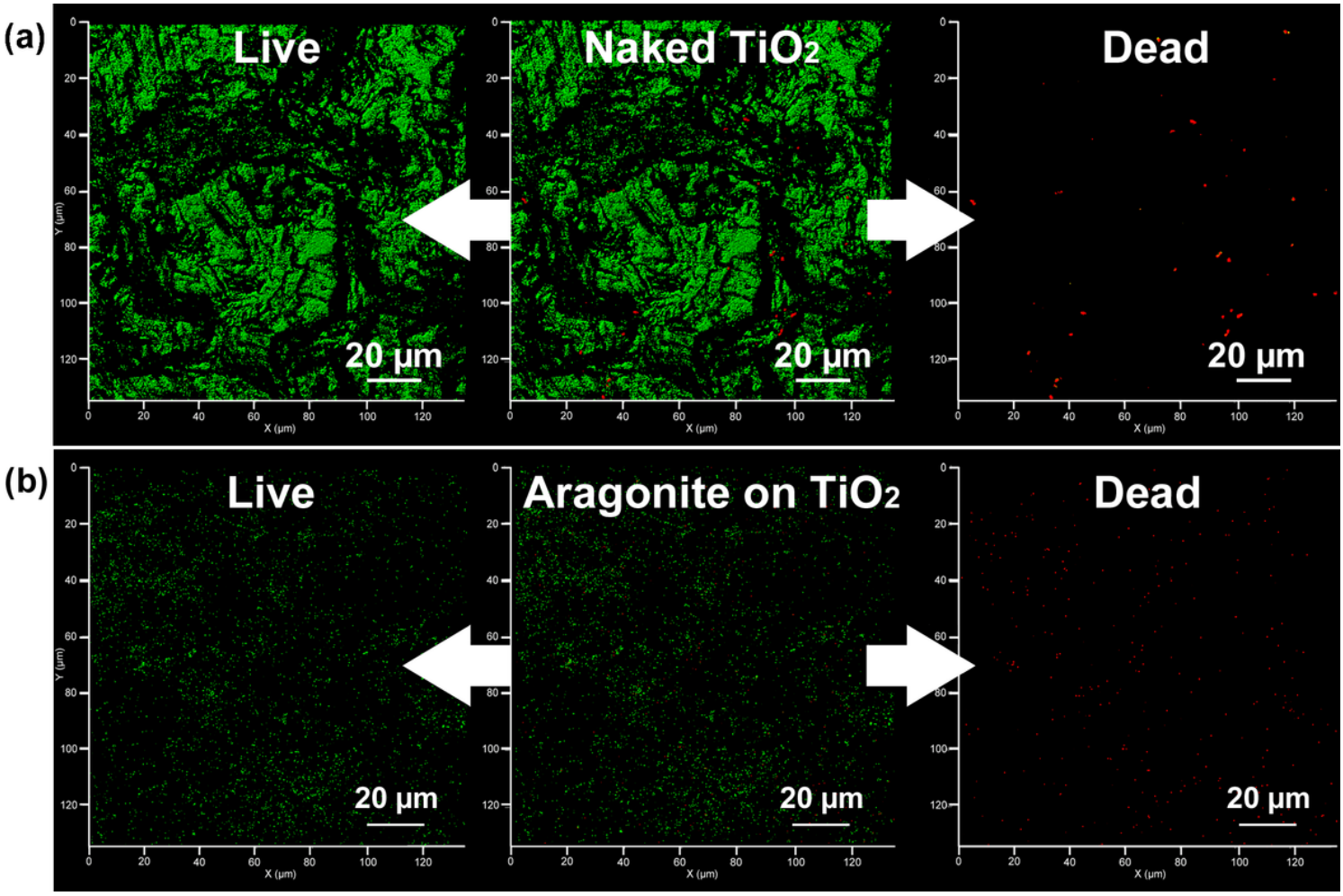


## Figure 6

Confocal microscopy image of stained E. coli K-12 cells on an unmodified TiO2 ceramic surface (a) and an aragonite-modified TiO2 ceramic surface (b).

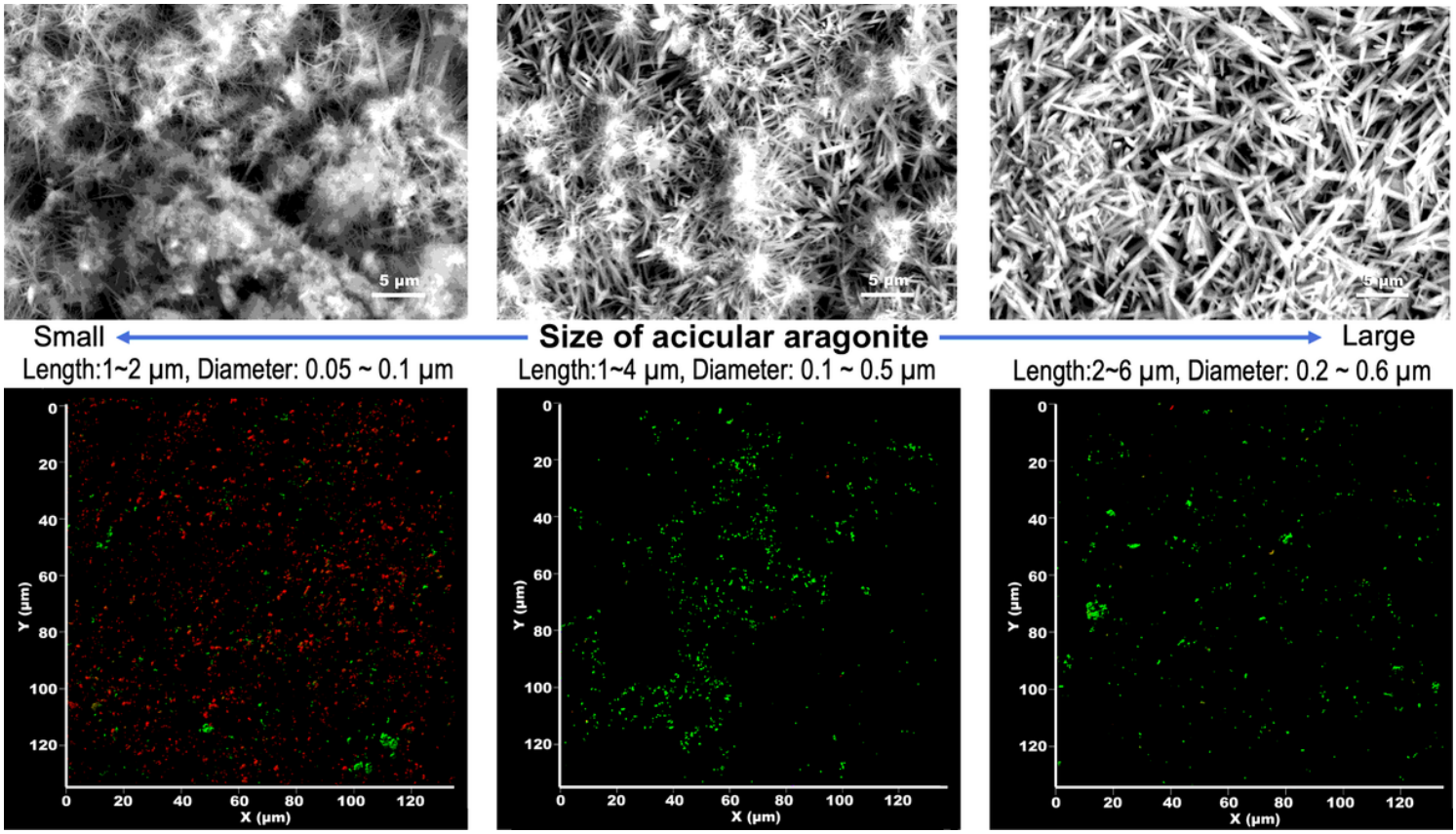


## Figure 7

Relationship between the crystal size of acicular aragonite and bactericidal performance. The mechano-bactericidal performance of acicular aragonite decreases with increasing crystal size. The bioactive cells remain in the aqueous phase except in the finely textured acicular aragonite system.

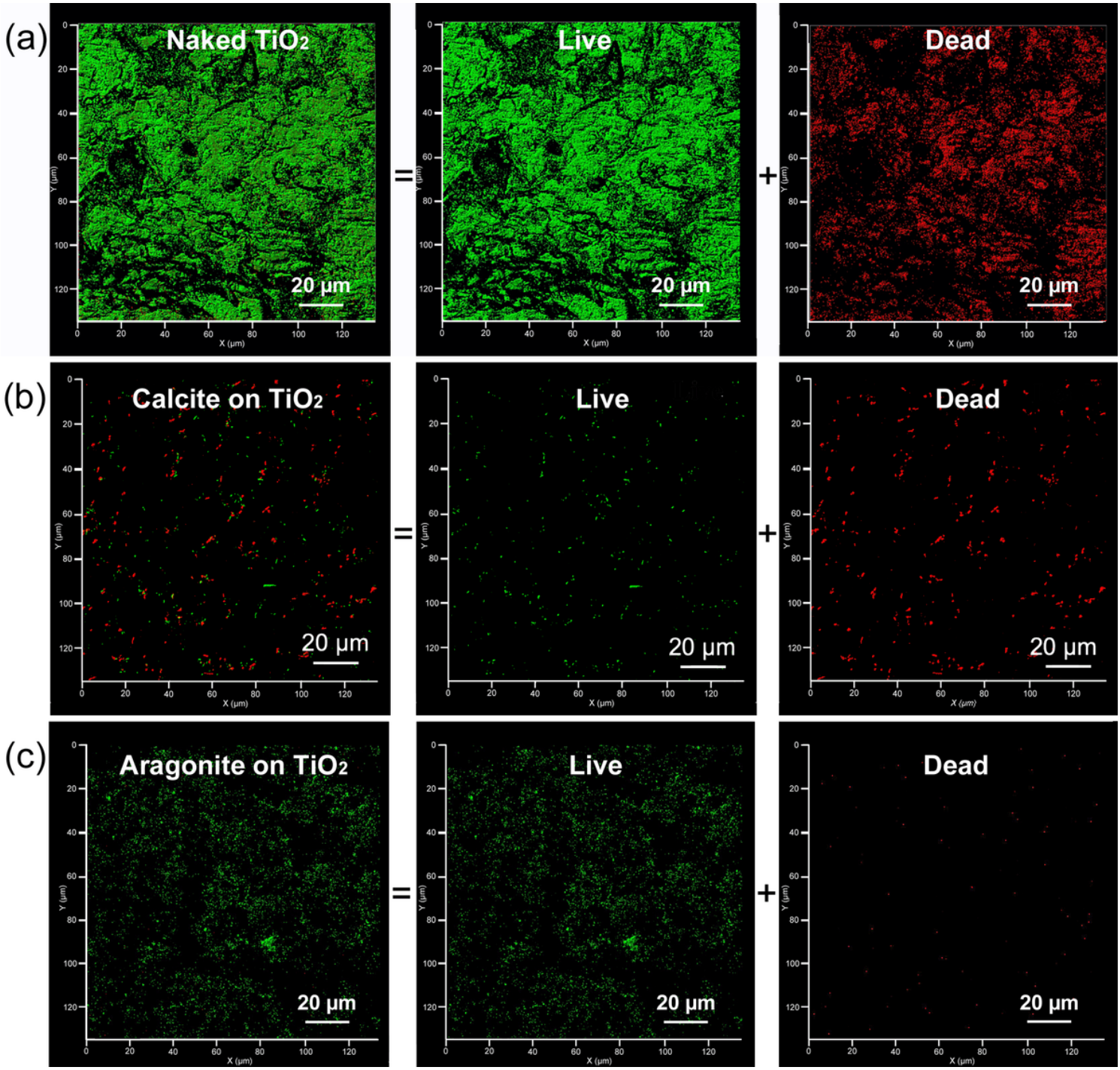


## Figure 8

Observations of mechano-bactericidal effects in circulation systems. (a) Confocal microscopy images of stained E. coli K-12 cells on an unmodified TiO2 ceramic surface. Live and dead cells are equally distributed on the TiO2 surface. (b) Confocal microscopy image of stained E. coli K-12 cells on a calcite-modified TiO2 ceramic surface. (c) Confocal microscopy image of stained E. coli K-12 cells on an aragonite-modified TiO2 ceramic surface.

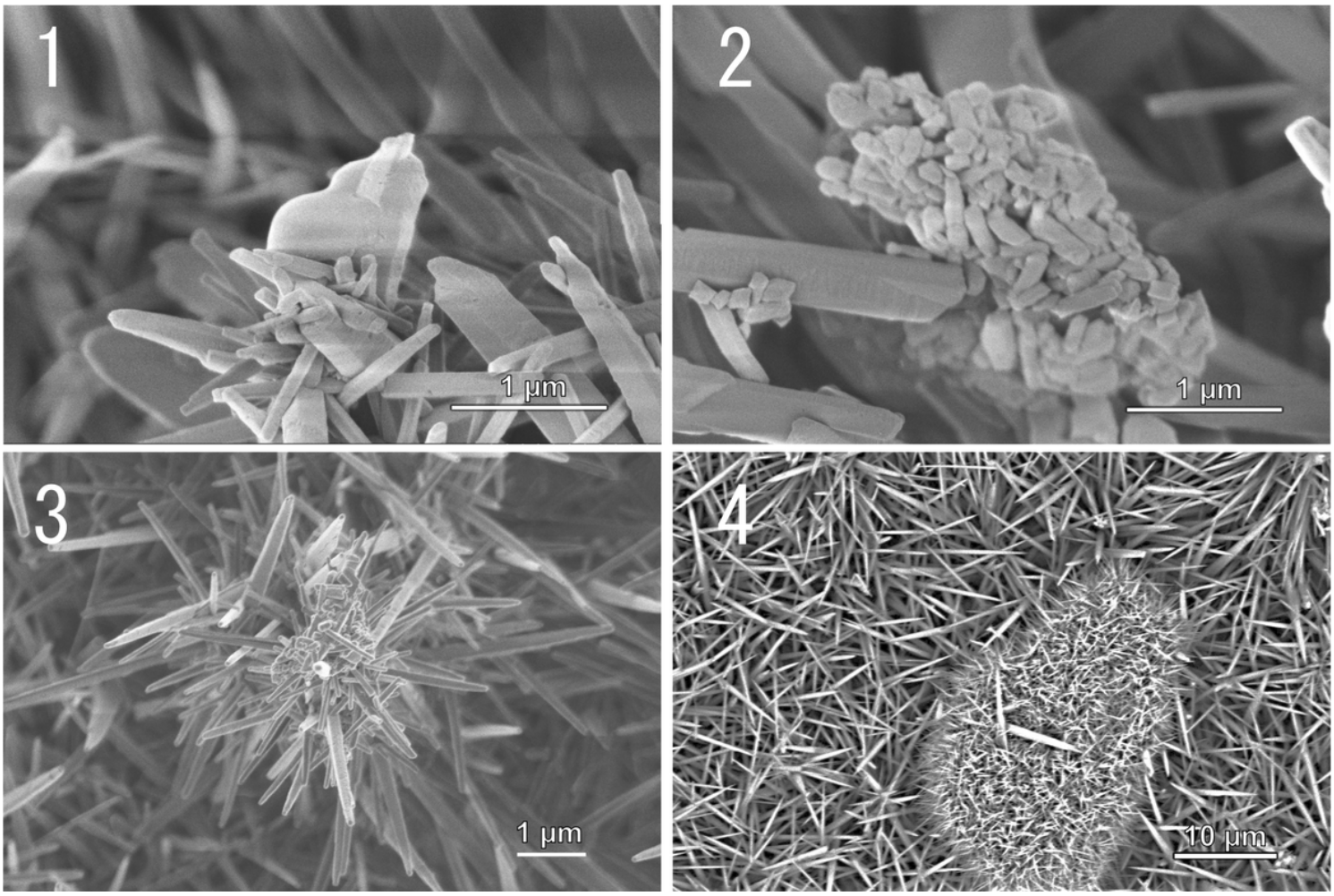


**Figure 9**

Surface of acicular aragonite-modified TiO2 ceramic after three weeks of exposure to circulating mineral water containing E. coli K-12. A cell membrane fragment of a dead cell is observed and aragonite crystals have started to grow on its surface (1). Aragonite crystals start to grow and cover the surfaces of dead cells (2). The growth of aragonite crystals is stimulated by the circulating mineral water, resulting in the large acicular crystals observed (3). A cluster of dead bacterial cells covered by acicular aragonite (4).

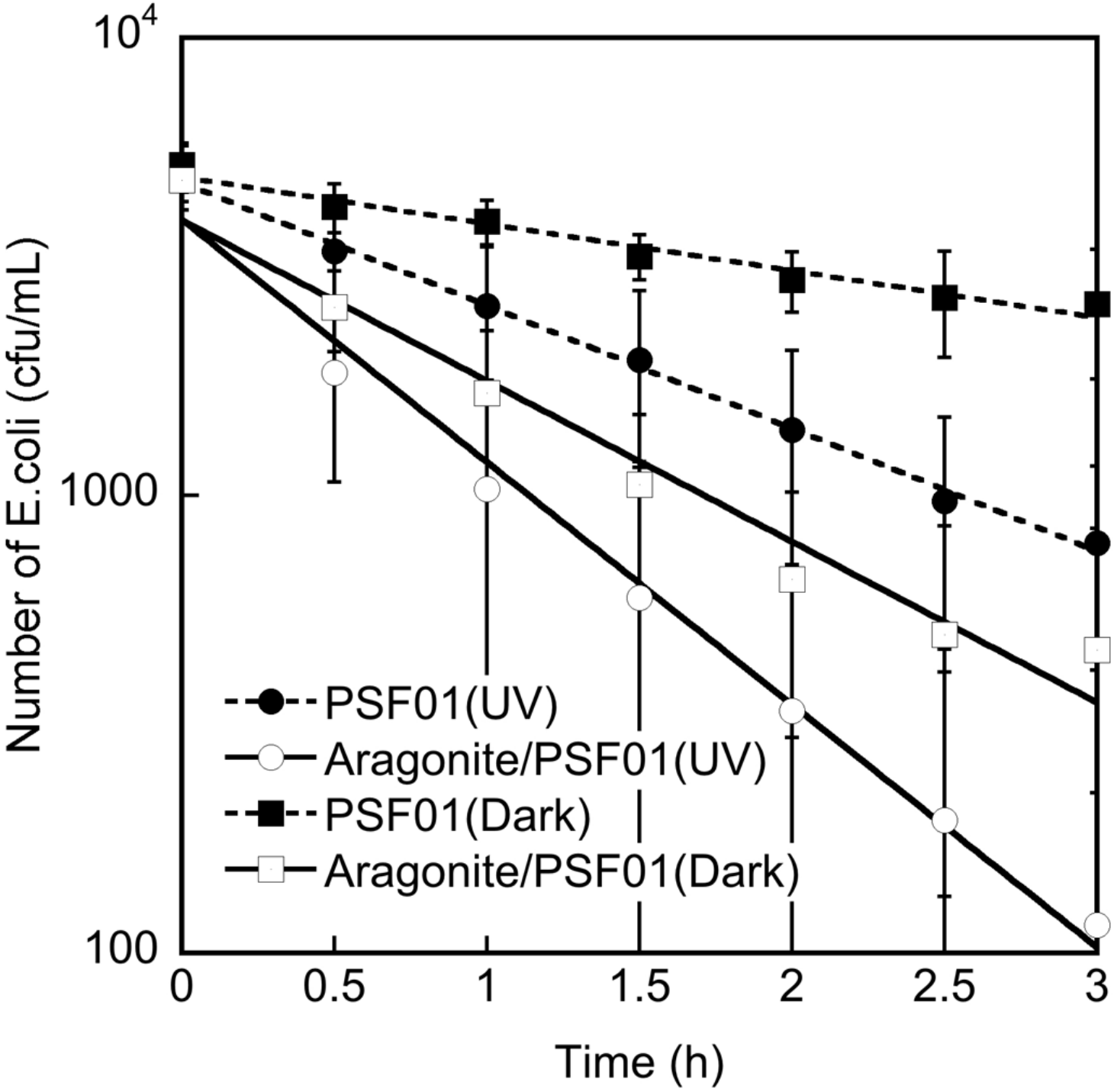


**Figure 10**

Change in the number of E. coli K-12 cells over time in circulation systems featuring unmodified and aragonite-modified TiO2 ceramics under dark and UV light conditions.